Iranian Society of Acoustics and Vibration
The 15th ISAV2025 International Conference on Acoustics and Vibration
24-25 Dec 2025 Tehran- Iran

Enhanced Acoustophoresis Size-Selective Particle Manipulation Utilizing Ridge-included Acoustofluidics

Negar Alamdari, Behdad Barahimi, Elahe Hosseini, Sara Darbari, Mohammad Kazem Moravvej-Farshi

School of Electrical and Computer Engineering, Tarbiat Modares University, Tehran 14115-111, Iran

- ** Corresponding author e-mail:* moravvej@modares.ac.ir , s.darbari@modares.ac.ir

Abstract

A ridge-included standing surface acoustic wave (SSAW) acoustofluidic device is developed for size-selective manipulation of microparticles. The system consists of interdigital transducers (IDTs) on a $LiNbO_3$ substrate and a PDMS microchannel integrated with SU-8 micro-ridge resonators that locally amplify the acoustic fields. Operating at 9.87 MHz, the device was tested using 0.2, 0.5, and 2.5 µm polystyrene particles under flow rates of 1,2 and 5 µL min^{-1} and voltages up to 15 V. Results show tunable size-dependent manipulation governed by acoustic forces, sample flow rates, and applied RF signal voltages. Submicron particles trapped up to 60% in vortical paths at 1 µL min^{-1} flow rate, whereas few micron-sized particles were trapped along with efficiencies up to 82% even at 5 µL min^{-1} flow rate. The ridge-assisted acoustofluidic device enhances field and energy localization, providing an inspiring approach for bio-particle focusing and manipulation in lab-on-a-chip applications.

Keywords: Standing Surface Acoustic Wave; Acoustofluidics; Ridge-included; Sub-micron Particle, Acoustic Fields Enhancement.

1. Introduction

Micron/submicron particles and cells manipulation plays a vital role in biomedical diagnostics, tissue engineering, and lab-on-a-chip technologies. Several contactless approaches—such as optical, electrical, magnetic, and acoustic tweezers—have been developed to manipulate microscopic objects suspended in fluids [1–3]. Among these, acoustofluidics, which combines microfluidics with acoustic actuation, has emerged as a powerful technique owing to its label-free operation, low power requirement, and high biocompatibility [3–5]. In acoustofluidics, the motion of suspended particles is primarily governed by two major effects: the acoustic radiation force (ARF) and the acoustic induced drag force (AIDF) [5–7]. The dominance of each force depends on particle size, fluid viscosity, and the acoustic frequency [1-3-7]. When the particle radius exceeds a critical value, ARF dominates and drives particles toward pressure nodes or antinodes of a standing wave; smaller particles, however, experience stronger acoustic-induced drag force from streaming vortices [6–8].

Standing surface acoustic waves (SSAWs), generated by the interference of two counter-propagating surface acoustic waves on a piezoelectric substrate, have been widely used for particle focusing, trapping, and patterning [4, 9, 10].

Conventional acoustofluidic systems are limited by their working frequency and require relatively high-power RF signal to efficiently influence submicron particles. Moreover, the standard interdigital-transducers (IDTs) geometry has limited capability to localize or amplify the acoustic field within the fluid microchannel. To overcome these challenges, local field-enhancement strategies employing micro- and nano-structures have recently been proposed [1, 2, 6, 11]. Sharp-edged or resonant microstructures can confine acoustic energy to sub-wavelength regions, significantly increase local pressure and velocity gradients [1, 2, 6]. In particular, surface-coupled resonant ridges have demonstrated reinforced acoustic forces and vortex formation near ridge edges, enabling efficient manipulation with reduced power consumption [2]. Despite such progress, experimental demonstrations of SSAW-driven local resonant amplification for selective particle manipulation remain scarce.

In this work, we present a $LiNbO_3$-based SSAW acoustofluidic platform integrated with SU-8 ridge resonators designed to enhance local acoustic fields for size-selective particle manipulation. The ridge structures amplify pressure and velocity gradients, generating strong local vortices and radiation-force potentials that provide trapping near ridge edges. Experiments using polystyrene particles of 0.2, 0.5 and 2.5 µm radius under various flow rates and voltages confirm tunable size-dependent particle manipulation of our ridge-included acoustofluidic device. These results demonstrate a compact and low-power ridge-enhanced acoustofluidic device capable of precise and tunable particle manipulation for future lab-on-a-chip applications.

2. Theoretical background

When an alternating voltage is applied to the interdigital transducers (IDTs) patterned on a piezoelectric substrate, periodic mechanical deformation occurs due to the inverse piezoelectric effect, generating a surface acoustic wave (SAW). The acoustic wavelength (λ) is determined by the IDT pitch and the substrate's Rayleigh wave Velocity v_{sub} , as:

$$f = \frac{v_{sub}}{\lambda} \tag{1}$$

In standing surface acoustic wave (SSAW) devices, two counter-propagating SAWs of identical frequency interfere, forming a stationary pattern of pressure nodes and antinodes along the microchannel. When the wave couples into the liquid domain at an angle known as the Rayleigh angle (θ_R), given by:

$$\theta_R = \sin^{-1}\frac{c_f}{c_s} \tag{2}$$

leaky waves propagate into the fluid, inducing both acoustic pressure fields and steady vortical motion (acoustic streaming) [5,7]. The time-averaged acoustic radiation force (ARF) acting on a spherical particle suspended in a viscous medium can be expressed as:

$$F_{ARF} = -(\frac{\pi P_0^2 V_P k_0}{2\lambda})\phi(k,\rho)\sin(\frac{4\pi X}{\lambda}) \tag{3}$$

For a sinusoidal SSAW propagating along the *x*-axis, this one-dimensional form describes the spatial variation of the acoustic potential field. Here, P_0 is the acoustic pressure amplitude, V_P is the particle volume, k_0 is the acoustic wavenumber, and λ is the wavelength. The term $\phi(k,\rho)$ is the acoustic contrast factor, which depends on the ratio of compressibility and density between the particle and the surrounding medium. The sign of ϕ determines whether the particle migrates toward the pressure nodes $(\phi \succ 0)$ or antinodes $(\phi \prec 0)$.

In parallel, the acoustic drag–induced force (ADIF) resulting from streaming flow is expressed as [5]:

$$F_{AIDF} = 6\pi\eta a(V_2 - V_0) \tag{4}$$

where η is the fluid viscosity, and V_2 is the streaming velocity. The overall particle trajectory is determined by the balance between F_{ARF} and F_{AIDF}, which defines a critical radius a_c separating radiation- and drag-dominated regimes. The relative dominance of acoustic radiation and drag-induced forces depends strongly on the particle size. For larger particles, the radiation force F_{ARF} governs the migration toward pressure nodes, whereas smaller particles are more influenced by streaming-induced drag F_{AIDF}, following the local vortical flow patterns, as shown in Figs. 1(a) and 1(b).

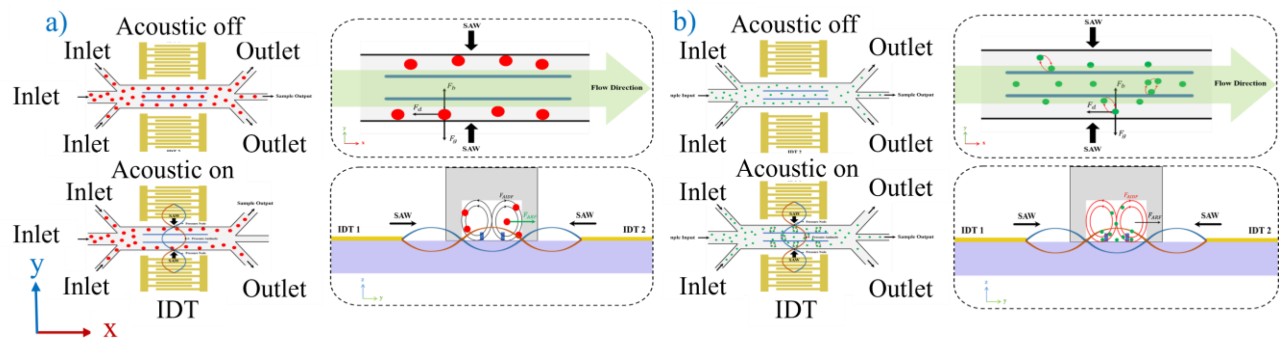

Fig. 1. *Schematic illustration of the force mechanisms in an SSAW acoustofluidic device. (a) For larger particles ($a > a_c$), the acoustic radiation force F_{rad} dominates, driving particles toward pressure nodes along the standing wave pattern. (b) For smaller particles ($a < a_c$), the streaming-induced drag force F_{ADIF} prevails, causing circulation around vortices near ridge edges and within the microchannel.*

3. Device design and Fabrication

The proposed acoustofluidic device was designed to generate a one-dimensional standing surface acoustic wave (SSAW) within a PDMS microchannel integrated on a $LiNbO_3$ substrate. The device employs a pair of interdigital transducers (IDTs) patterned symmetrically on both sides of the channel. Each IDT includes ten pairs of Ti/Au electrodes with a finger pitch of 400 µm, corresponding to a resonance frequency of approximately 9.9 MHz. The piezoelectric substrate thickness was 500 µm to ensure efficient wave propagation and minimal acoustic attenuation. The PDMS microchannel, fabricated by standard soft-lithography, had a width of 200 µm, height of 80 µm, and length of 7 mm. On the channel floor, SU-8 micro-ridges with a height of about 10 µm were patterned at a 30 µm offset from the channel centerline. These ridges act as local acoustic resonators that concentrate the pressure and velocity fields, thereby amplifying the effective acoustic radiation and streaming forces applied to the suspended particles. Fabrication of the $LiNbO_3$-based chip followed standard photolithography and lift-off processes. First, the substrate was cleaned with acetone, isopropanol, and deionized water, followed by dehydration baking. A photoresist layer was spin-coated, exposed through a chrome mask, and developed to define the IDT pattern. A thin titanium layer (10 nm) and a gold layer (100 nm) were deposited using sputtering. The lift-off process in acetone left clean, well-aligned electrodes on the substrate surface .After electrode formation, SU-8 (type 2010) was spin-coated over the channel region and processed by UV exposure and development to form periodic ridge structures. A PDMS microchannel was then molded using a master pattern, cured at 70 °C, and aligned to the patterned substrate. The PDMS layer was permanently bonded to the $LiNbO_3$ chip after oxygen plasma activation, creating a sealed microchannel that ensures efficient acoustic coupling between the substrate and fluid. This configuration enables reliable generation of SSAW fields with locally reinforced acoustic energy, forming a compact and robust platform for efficient particle manipulation and separation.

4. Experimental setup and operation

After fabrication, the PDMS microchannel was bonded onto the $LiNbO_3$ substrate and connected to inlet and outlet tubes for sample injection. The assembled SSAW chip was mounted on a printed circuit board (PCB) for stable electrical connection to the IDTs. Wires were attached to the gold pads using conductive silver paste, as shown in Fig. 2(b). The complete device and its schematic representation are presented in Fig. 2(a–c).

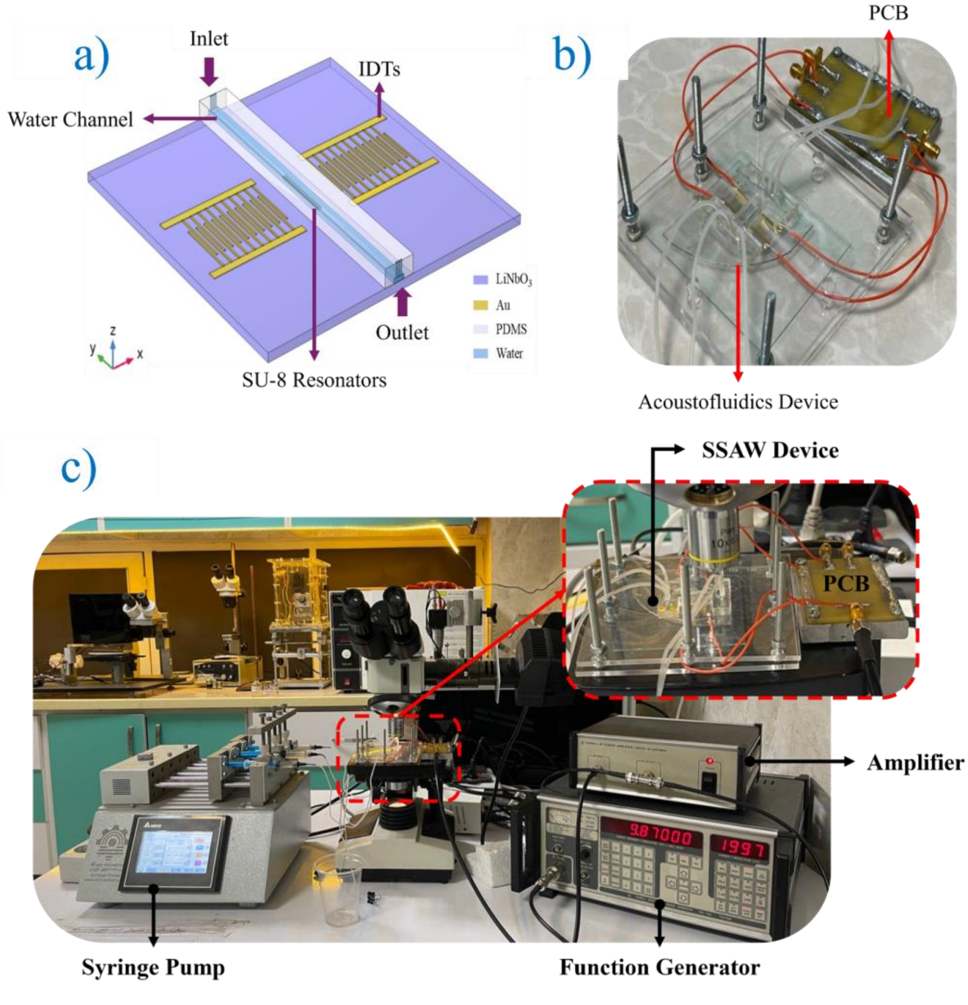

Fig. 2. *(a) Schematic of the SSAW acoustofluidic device showing IDTs, PDMS microchannel, and SU-8 resonators. (b) Photograph of the fabricated device with electrical connections and PDMS layer. (c) Experimental setup showing the syringe pump, optical microscope, function generator, RF amplifier, and PCB used for SSAW excitation and particle-tracking experiments.*

The experimental setup (Fig. 3c) consisted of a function generator (Agilent 33120A) producing sinusoidal signals at the resonance frequency (~9.87 MHz), connected to a 20 dB RF amplifier (Mini-Circuits ZHL-20W-13+) to drive the IDTs. A syringe pump (NewEra NE-1000) delivered particle suspensions at controlled flow rates of 1, 2, and 5 µL min⁻¹ through the channel. The voltage amplitude was varied between 0 and 15 V to study the influence of acoustic power on particle motion. Observations were made using an optical microscope equipped with a high-speed camera for video capture and subsequent particle-tracking analysis.

5. Results and Discussion

To evaluate the acoustofluidic performance of the ridge-enhanced SSAW device, the migration dynamics of polystyrene (PS) particles with diameters of 0.2 µm, 0.5 µm, and 2.5 µm were characterized under different flow rates and excitation voltages. The resonance frequency of 9.87 MHz was applied to the IDTs, and the lateral velocity of particles across the microchannel was extracted from sequential video frames using image-tracking analysis.

5.1 A. Lateral Velocity Characterization

Figures 3(a–c) illustrate the variation of average lateral velocity for 0.2 µm, 0.5 µm, and 2.5 µm polystyrene particles as functions of applied voltage and flow rate. For all particle sizes, the velocity increased with voltage, confirming that stronger acoustic excitation generates more intense streaming vortices within the microchannel. At 0 V, the motion of particles followed purely hydrodynamic flow with negligible lateral displacement. All tested particles are smaller than the critical radius a_c, and their motion is therefore dominated by the acoustic drag-induced force F_{AIDF} associated with streaming. However, as the particle size increases, the acoustic forces acting on them become more pronounced due to their larger volume and stronger interaction with the pressure field. Consequently, smaller particles such as the 0.2 µm ones exhibit the highest lateral velocity (~35 µm s^{-1} at 15 V and 2 µL min^{-1}), driven by vigorous circulation near the SU-8 ridge edges. For 0.5 µm particles, the lateral velocity decreases as their response to streaming weakens. In the case of 2.5 µm particles, although still below the critical radius, they experience stronger acoustic influence, which confines them closer to the ridge regions where the acoustic field is most intense. This confinement leads to reduced effective displacement and lower average lateral velocity compared to smaller particles.

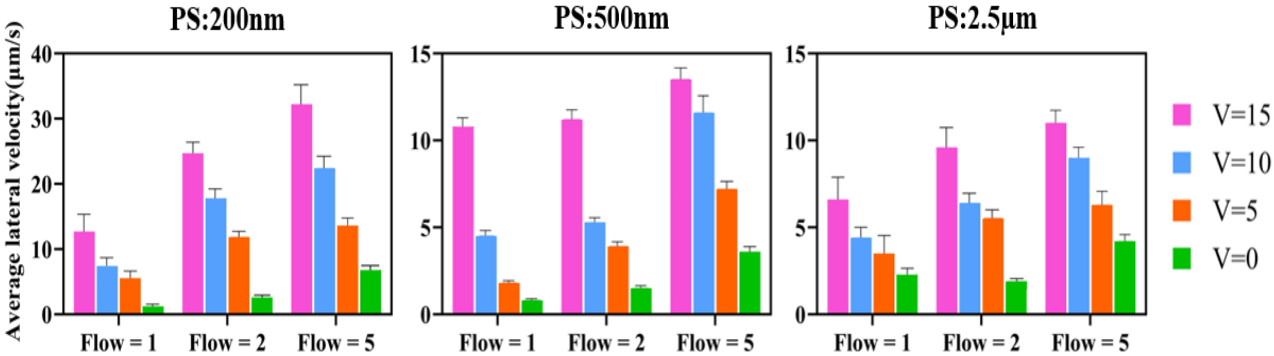

Fig. 3. *(a–c) Average lateral velocity of 0.2 µm, 0.5 µm, and 2.5 µm polystyrene particles as a function of flow rate and applied voltage. Each data point represents the mean of multiple trajectories with standard deviation error bars.*

5.2 Trapping Efficiency Analysis

To further quantify acoustic performance, the trapping efficiency (defined as the percentage of particles confined near the node region within a fixed observation window) was calculated for different flow rates (Fig. 4).

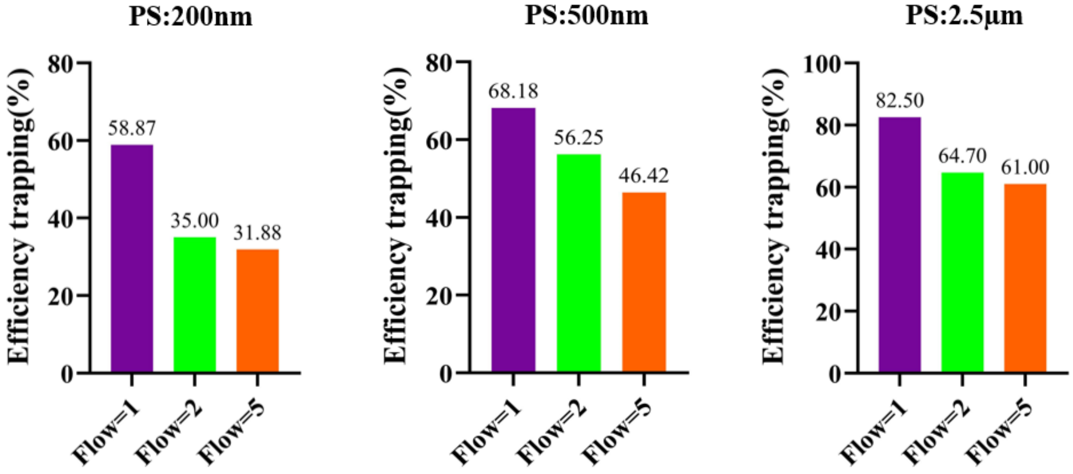

Fig. 4. *Trapping efficiency of polystyrene particles (0.2, 0.5 and 2.5 μm) at different flow rates under 15V excitation. Larger particles exhibit higher efficiency due to the dominance of acoustic radiation forces*.

At a constant voltage of 15 V, the trapping efficiency decreased with increasing flow rate for all particle sizes due to reduced residence time within the acoustic field. For 0.2 µm particles, efficiency declined from ~59 % at 1 µL min^{-1} to ~32 % at 5 µL min^{-1}, reflecting dominance of streaming drag. For 0.5 µm particles, efficiency reached ~68 % at low flow and dropped to ~46 % at high flow, showing a mixed regime. The 2.5 µm particles demonstrated the highest efficiency (up to ~83 %), confirming that larger particles are strongly influenced by F_{rad} and tend to aggregate near ridge edges where local acoustic intensity is maximum.

5.3 Discussion

The overall results validate that the interplay between radiation and drag forces governs particle behavior in SSAW microchannels. Sub-micron particles are primarily transported by streaming vortices, whereas micron-scale particles undergo radiation-dominated focusing toward nodes. The introduction of SU-8 ridges resonators significantly enhanced local acoustic fields, resulting in higher velocities and trapping efficiencies compared to conventional planar SSAW devices reported in literature [2, 6]. The dependence on particle size, flow rate, and input power observed here aligns with theoretical predictions (Section II) and confirms that localized field reinforcement can be exploited for selective manipulation. The ridge-enhanced SSAW platform therefore offers a tunable and energy-efficient route for on-chip sorting of biological cells and sub-micron particles.

6. List of references

[1] W. S. Harley, K. Kolesnik, M. Xu, D. E. Heath, and D. J. Collins, "3D Acoustofluidics via Sub-Wavelength Micro-Resonators," *Adv. Funct. Mater.*, vol. 33, p. 2211422, 2023.

[2] B. Barahimi, S. Darbari, M. Zabetian Targhi, I. Halvaei, and R. Nosrati, "Surface-Coupled Locally Resonant Modes for Reinforced and Localized Acoustofluidic Particle Manipulation," *Phys. Fluids*, vol. 37, p. 021916, 2025.

[3] Z. Wang, J. Xia, R. Garry, D. A. Weitz, and X. Li, "Recent Progress on Acoustofluidic Manipulation of Cells and Particles," *Natl. Sci. Open*, vol. 4, p. 20230080, 2025.

[4] J.-C. Hsu, C.-H. Hsu, and Y.-W. Huang, "Acoustophoretic Control of Microparticle Transport Using Dual-Wavelength Surface Acoustic Wave Devices," *Micromachines*, vol. 10, p. 52, 2019.

[5] P. B. Muller, R. Barnkob, M. J. H. Jensen, and H. Bruus, "A Numerical Study of Microparticle Acoustophoresis Driven by Acoustic Radiation Forces and Streaming-Induced Drag Forces," *Lab Chip*, vol. 12, pp. 4617–4627, 2012.

[6] W. S. Harley, K. Kolesnik, D. E. Heath, and D. J. Collins, "Enhanced Acoustic Streaming Effects via Sharp-Edged 3D Microstructures," *Lab Chip*, vol. 24, pp. 1626–1635, 2024.

[7] J. Friend and L. Y. Yeo, "Microscale Acoustofluidics," *Rev. Mod. Phys.*, vol. 83, pp. 647–704, 2011.

[8] H. Bruus, "Acoustofluidics 7: The Acoustic Radiation Force on Small Particles," *Lab Chip*, vol. 12, pp. 1014–1021, 2012.

[9] Y. Ai, M. K. Zhu, and T. Laurell, "Standing Surface Acoustic Wave Based Microfluidic Sorting," *Anal. Chem.*, vol. 83, pp. 7428–7433, 2011.

[10] T. Laurell, F. Petersson, and A. Nilsson, "Particle Separation in Microfluidics Using Standing Surface Acoustic Waves," *Proc. IEEE Ultrason. Symp.*, pp. 1645–1648, 2014.

[11] X. Li *et al.*, "Localized Acoustic Field Engineering for Microscale Manipulation," *Natl. Sci. Open*, vol. 4, 2025.